Chemical Engineering Science 124 (2015) 27–36

Contents lists available at ScienceDirect

Chemical Engineering Science

journal homepage: www.elsevier.com/locate/ces

Amine-modified Mg-MOF-74/CPO-27-Mg membrane with enhanced H_2/CO_2 separation

Nanyi Wang [a], Alexander Mundstock [a], Yi Liu [a], Aisheng Huang [b,*], Jürgen Caro [a,*]

[a] Institute of Physical Chemistry and Electrochemistry, Leibniz University Hannover, Callinstr. 22, D-30167 Hannover, Germany
[b] Institute of New Energy Technology, Ningbo Institute of Material Technology and Engineering, CAS, 1219 Zhongguan Road, 315201 Ningbo, PR China

HIGHLIGHTS

- Amination of the open metal sites in Mg-MOF-74 leads to retardation of CO_2 and doubles the selectivity for H_2/CO_2 separation.
- The size of Mg-MOF-74 crystals in membrane can be reduced after optimization of synthesis solution.
- Only by using MgO as seeds, a dense and continuous Mg-MOF-74 layer could be obtained.
- The selectivity of the Mg-MOF-74 membrane for H_2/CO_2 is far above the Robeson bound.

GRAPHICAL ABSTRACT

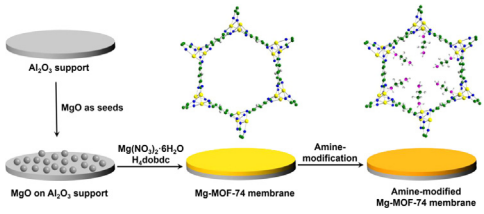

ARTICLE INFO

Article history:
Received 8 October 2014
Received in revised form
17 October 2014
Accepted 20 October 2014
Available online 27 October 2014

Keywords:
Metal–organic framework
Mg-MOF-74 membrane
Amine-modification
Gas separation

ABSTRACT

Mg-MOF-74 has attracted intense attention due to its high CO_2 uptake ability. In this work, a new strategy by using magnesium oxide as seeds was developed to synthesize a dense, defect-free Mg-MOF-74 membrane with hydrogen-selectivity. The mixed gas separation factor of H_2/CO_2 mixture could be improved by the post-modification of the Mg-MOF-74 membrane with ethylenediamine, since the modification with amine groups enhanced the strong adsorption of CO_2 molecules, which reduces the permeance of CO_2. The separation factors for both as-synthesized and amino-functionalized Mg-MOF-74 membranes reduce gradually with increasing temperature. After amination of the open Mg sites, the separation performance of the Mg-MOF-74 membrane was remarkably enhanced, and the H_2/CO_2 selectivity increased from 10.5 to 28 at room temperature.

1. Introduction

As a high-quality and clean energy carrier, hydrogen has attracted renewed and increasing attention around the world in recent years. Currently, the majority of hydrogen is produced by steam-methane reforming (SMR) followed by a water-gas shift (WGS) strategy. Before hydrogen can be used in fuel cell, it has to be purified from the resulting SMR gas mixture which mainly contains CO_2. Also in the pre-combustion technology of CO_2 sequestration, H_2-selective membranes are desired. In the case of pre-combustion CO_2 capture, H_2-selective membranes can be applied at moderate temperatures (150–250 °C) in a one-step separation process. This approach offers the advantages that (i) the mixture of CO_2 and H_2 has already a high pressure, and that (ii) the application of selective H_2-permeable membranes can deliver CO_2 at high pressure, thus reducing compression costs. Therefore, the separation of H_2 from CO_2 is of high interest. Compared with conventional separation methods such as pressure swing adsorption (PSA), membrane separation is the most promising alternative because of its low energy consumption, ease of operation, and cost effectiveness (Rostrup-Nielsen and

* Corresponding authors. Tel.: +49 511762 3175; fax: +49 511 762 1912.
E-mail addresses: huangaisheng@nimte.ac.cn (A. Huang), juergen.caro@pci.uni-hannover.de (J. Caro).

http://dx.doi.org/10.1016/j.ces.2014.10.037
0009-2509/

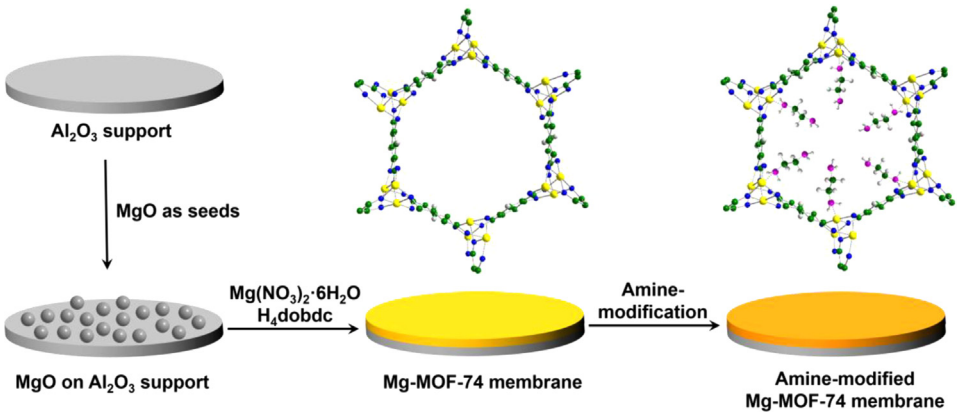

Fig. 1. Scheme of the synthesis of Mg-MOF-74 membrane on MgO-seeded Al_2O_3 supports and amine-modification of the as-prepared Mg-MOF-74 membrane.

Rostrup-Nielsen, 2002; Brown et al., 2014; Rodenas et al., 2014). Inorganic membranes like zeolites, Pt-alloys and carbon are of special interest since – different to organic polymer membranes – they can be operated under harsh separation conditions. In the recent 20 years, various hydrogen permselective inorganic membranes have been developed for the separation of H_2 from CO_2 (Shiflett and Foley, 1999; Uemiya et al., 1991; Ockwig and Nenoff, 2007; de Vos and Verweij, 1998; Hong et al., 2008; Huang et al., 2010). However, the preparation of highly H_2-permselective membranes is still a challenge.

Metal–organic frameworks (MOFs), which consist of metal ions or metal oxide clusters interconnected by anionic organic linkers, have attracted intense attention for potential applications in catalysis, separation, gas adsorption and gas storage due to their well-defined pore structure and specific adsorption affinities. (Yaghi et al., 2003; Seo et al., 2000; Ranjan and Tsapatsis, 2009; Lu and Hupp, 2010; Hermes et al., 2005; Zhao et al., 2009; Yoo et al., 2009; Li et al., 2010; Huang et al., 2012; Liu et al., 2013) Magnesium dioxybenzenedicarboxylate (Mg-MOF-74 or Mg/dobdc, also known as CPO-27-Mg, hereafter termed Mg-MOF-74) (Rosi et al., 2005), one of the iso-structural compounds of $M_2(dhtp)(H_2O)_2 \cdot 8H_2O$ (M-MOF-74, M=Ni, Co, Zn, Mg, Mn, dhtp=dihydroxyterephthalic) (Dietzel et al., 2005, 2008, 2006; Britt et al., 2009) is under intense investigation due to its significantly high CO_2 adsorption capacities. (Ranjan and Tsapatsis, 2009; Dietzel et al., 2009) Mg-MOF-74 is built up by the linkage of the Mg^{2+} ions with 2,5-dioxido-1,4-benzenedicarboxylate (DOBDC), where the metal ions build a distorted octahedron and the carboxylate groups act as ligand of the metal cations, to form a well-defined hexagonal, one-dimensional (1D) pore structure with a pore diameter of about 11 Å (Caskey et al., 2008; Bétard et al., 2010).

Attributing to the unique feature of its framework structure, where metal cations are bonded with five oxygen atoms to form a square-pyramid coordination, and the unsaturated metal sites in the center of the square plane are free to interact with CO_2 molecules, Mg-MOF-74 has a high CO_2 adsorption capacity (380 mg CO_2/g at room temperature under dry conditions) (Yazaydin et al., 2009). Due to its high gas adsorption ability, many studies have been focused on the gas separation efficiency of Mg-MOF-74 (Mason et al., 2011; Yang et al., 2012; Dietzel et al., 2010; Herm et al., 2012; Yu and Balbuena, 2013; Böhme et al., 2013; Mundstock et al., 2013).

Although there are numerous of studies of Mg-MOF-74 powders on the gas adsorption incl. simulation (Kong et al., 2012; Dzubak et al., 2012; Remy et al., 2013), to date no Mg-MOF-74 membrane with successful gas separation performance has been reported. In a first attempt, a supported Mg-MOF-74 membrane with a mean tilt angle of 31° of the 1D pore system from the direction perpendicular to the membrane surface could be developed (Mundstock et al., 2013). Lee et al. (2012) have prepared a Ni-MOF-74 membrane by using the layer-by-layer synthesis technique with a H_2/CO_2 selectivity of 9.1 at 25 °C. Bae and Long (2013) used Mg-MOF-74 nanocrystals in mixed-matrix membranes to improve the CO_2/N_2 selectivity of the polymer membrane. In the present work, we have developed a new strategy by using magnesium oxide as seeds to synthesize a dense, defect-free Mg-MOF-74 membrane for gas separation. Moreover, the post-synthesis modification with ethylenediamine, which was developed by Choi et al. (2012), was employed to improve its gas separation efficiency (Fig. 1). When preparing supported MOF membranes with a 1D pore system, the orientation of the pores in a suitable direction remains a challenge as addressed for the first time for the Mn formate membrane (Arnold et al., 2007).

2. Experimental

2.1. Materials

Chemicals were used as received. 2,5-dihydroxyterephthalic acid (H_4dobdc, 98%, Aldrich), magnesium nitrate hexahydrate (99%, Sigma-Aldrich), magnesium oxide (99.9%, ChemPur), polyethyleneimine (branched, avg MW~25000 by LS, Aldrich), ethylenediamine (≥ 99%, Sigma-Aldrich), toluene (≥ 99.8%, Acros), *N*, *N*-dimethylformamide (DMF, water < 50 ppm, Acros), ethanol (≥ 99.8%, Sigma-Aldrich). Porous α-Al_2O_3 disks (Fraunhofer Institute IKTS, former HITK/Inocermic, Hermsdorf, Germany: 18 mm in diameter, 1.0 mm in thickness, 70 nm particles in the top layer) were used as supports.

2.2. Preparation of Mg-MOF-74 membranes

2.2.1. Seeding on the support surface

The seeding suspension was prepared by adding 1.5 g MgO and 1.2 g polyethyleneimine (PEI) in 100 mL water. PEI was used to ensure that the MgO particles (< 50 nm) adhered to the support surface. The suspension was then stirred overnight, and the α-Al_2O_3 supports were dipped in the seeding suspension by using an automatic dip-coating device with a dip- and withdraw-speed of 300 and 100 mm/min, respectively. The seeded supports were then air-dried at 100 °C overnight.

2.2.2. Synthesis of Mg-MOF-74 membrane

The Mg-MOF-74 membrane was prepared by a solvothermal reaction. $Mg(NO_3)_2 \cdot 6H_2O$ (0.2375 g, 0.925 mmol) and H_4dobdc (0.1011 g, 0.509 mmol) were added to a 15 mL solution which was

prepared by mixing DMF, water and ethanol with a volumetric ratio of 15:1:1. The MgO-coated supports were then placed vertically in a Teflon-lined stainless steel autoclave which was filled with the synthesis solution and then heated at 120 °C in an air-conditioned oven for 24 h. After solvothermal reaction, the Mg-MOF-74 membranes were washed with DMF three times, and then dried in air overnight.

2.2.3. Post-modification of the membrane

The as-prepared Mg-MOF-74 membranes were treated with ethylenediamine (0.5 g in 10 mL toluene) at 110 °C for 2 h under reflux in argon atmosphere. The membranes were then directly removed from the solution and dried in argon at room temperature.

2.3. Characterization

Scanning electron microscopy (SEM) micrographs were taken on a JEOL JSM-6700F with a cold field emission gun operating at 2 kV and 10 μA. The X-ray diffraction (XRD) patterns were recorded at room temperature under ambient conditions with Bruker D8 ADVANCE X-ray diffractometer with Cu$K\alpha$ radiation at 40 kV and 40 mA. FT-IR spectrums were recorded with a Tensor 27 instrument (Bruker) through KBr pellets using Ar/Xe laser line with $\lambda = 633$ nm.

2.4. Evaluation of single gas permeation and mixed gas separation

The as-prepared and amine-modified Mg-MOF-74 membranes synthesized on MgO-seeded α-Al_2O_3 supports at 120 °C for 24 h were evaluated by single gas permeation and mixture gas separation with Wicke–Kallenbach (Huang et al., 2010). For the measurements of gas separation performances, the supported Mg-MOF-74 membrane was sealed in a permeation module with silicone O-rings. The mounting of the membranes into the housing was done in a glove box under argon to avoid the influence of humid air. According to the Wicke–Kallenbach technique, on both sides of the membrane was atmospheric pressure, N_2 was used on the permeate side as sweep gas, except for the measurement of N_2 permeance where CH_4 was used as sweep gas. The flow rate on the feed side was kept constant for each gas with 50 mL min^{-1}, and the flow rate on the permeate side was kept at 50 mL min^{-1} as well. The fluxes of both the feed and sweep gas were controlled by mass flow controllers, and a calibrated gas chromatograph (HP6890) was used to detect the gas concentrations on the permeate side. The gas chromatograph (GC) was calibrated every week anew with standard gas mixtures. The accuracy of the GC analysis of our H_2/CO_2 mixture with TCD detection is about ±5 vol%. The permeance P is obtained by division of the flux by the transmembrane pressure difference, as shown in Eq.(1), where n is the amount of gas in mol, A is the membrane area, t is the permeation time, and Δp is the pressure difference. The separation factor $\alpha_{i,j}$ of a binary mixture permeation is defined as the quotient of the molar ratios of the components (i,j) in the permeate, divided by the quotient of the molar ratio of the components (i,j) in the retentate, as show in Eq. (2). Since less than 1% of the feed gas pass the membrane, the retentate composition is de facto identical with the feed composition.

$$P = \frac{n}{A \times t \times \Delta p} \tag{1}$$

$$\alpha_{i/j} = \frac{y_{i,perm}/y_{j,perm}}{y_{i,ret}/y_{j,ret}} \tag{2}$$

Originally, the Wicke–Kallenbach method has been developed for the determination of CO_2 surface diffusion with N_2 as sweep gas (Wicke and Kallenbach, 1941). It could happen therefore in our case that the adsorption of nitrogen on the permeate side of the membrane would falsify the separation factor, also the counter-diffusion of the sweep gas to the feed side can happen. Therefore, to prove the feasibility of the Wicke–Kallenbach technique, gas permeation measurements were also carried out without sweep gas. In one scenario, the feed side was at 1 bar, and the permeate side was at reduced pressure (vacuum). In another case, scenario 2, the pressure on the feed side was 2 bar, and the pressure on the permeate side was 1 bar. It was found that the fluxes of the components of the feed gases were increased in scenario 1 and decreased in scenario 2. This experimental finding can be understood by modified concentrations gradients over the membrane as driving force for permeation. However, the mixture separation factors kept almost unchanged (less than ± 5%).

We have also excluded another source of experimental errors. Before every gas permeation measurement, the membranes were first activated in situ at 100 °C by using 50 mL $min^{-1}H_2$ in the Wicke–Kallenbach permeation apparatus. All permeation data were collected in steady state of permeation after at least 5 h equilibration time. Sometimes, after 5 h equilibration time we waited for another 12 h. Since there was no change in the permeation data, we assume that the H_2/CO_2 mixed gas system was in steady state after 5 h.

The apparent activation energy E_{act} of permeation can be calculated according to the Arrhenius equation (Eq. (3)), where P_i is the permeance of component i, P_i^0 is the pre-exponential factor, R is the ideal gas constant (8.314 J mol^{-1} K^{-1}), and T is the temperature in Kelvin. Then E_{act} has been determined through the slope of the plot, which is obtained from the straight line of $\ln P_i$ against T^{-1} (Li et al., 2010) (see Section 3.4. Results of single gas permeation and mixture gas separation).

$$P_i = P_i^0 \exp\left(-\frac{E_{act}}{RT}\right) \tag{3}$$

3. Results and discussion

3.1. Effects of the synthesis solution on the membrane preparation

We first tried to grow a Mg-MOF-74 membrane following Caskey's recipe with a solution composition of 3.3 equiv. Mg $(NO_3)_2 \cdot 6H_2O$: 1 equiv. H_4dobdc (Caskey et al., 2008). However, we failed to prepare a continuous Mg-MOF-74 membrane after solvothermal synthesis for 24 h at 120 °C. As shown in Fig. 2(a), the crystals are too large to intergrow to a continuous layer, and big inter-crystalline gaps are easily observed in the Mg-MOF-74 layer. In order to control the size of the Mg-MOF-74 crystal and to avoid inter-crystalline voids, we modified the chemical composition of the synthesis solution by adjusting the ratio of Mg^{2+} and the $dobdc^{4-}$ linker. By use of the new recipe with a solution composition of 1.8 equiv. $Mg(NO_3)_2 \cdot 6H_2O$:1 equiv. H_4dobdc, the size of Mg-MOF-74 crystals can be remarkably reduced, and thus the crystals become well intergrown and form a dense Mg-MOF-74 membrane on the alumina support (Fig. 2(b)). XRD pattern of the Mg-MOF-74 membrane further confirms that the as-synthesized layer is a pure Mg-MOF-74 phase after the adjustment of the synthesis solution.

Due to the poor heterogeneous nucleation of Mg-MOF-74 crystals on the alumina support surface, it is difficult to form a continuous Mg-MOF-74 layer simply by in-situ hydrothermal synthesis. Fig. 3(a) shows the Mg-MOF-74 membrane prepared directly on the un-modified alumina support. It can be seen that the crystals don't grow into a dense membrane layer, and inter-crystalline gaps can be observed between the Mg-MOF-74 crystals. Therefore, we tried to improve their intergrowth by pre-coating

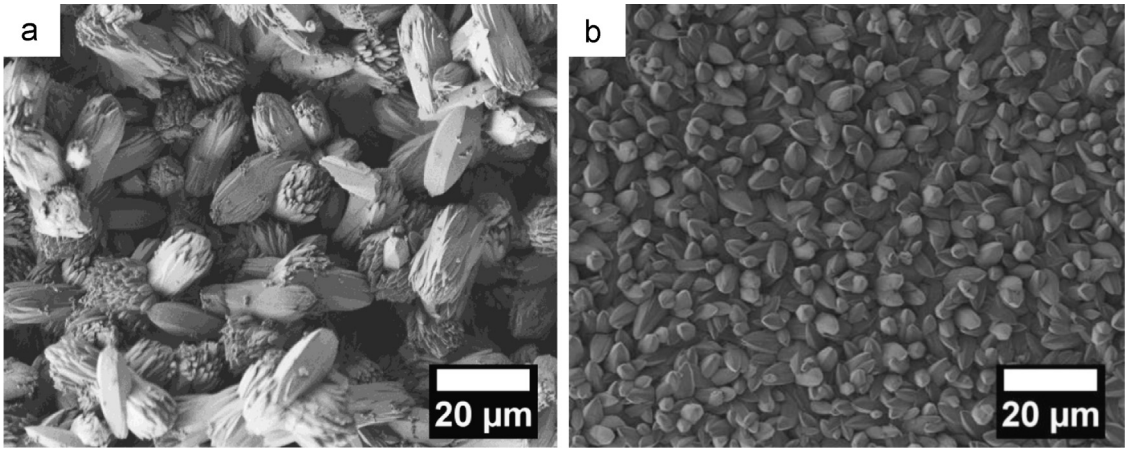

Fig. 2. Top view SEM images of Mg-MOF-74 membranes prepared on α-Al_2O_3 supports (a) before and (b) after the optimization of the synthesis solution (a cross-section of membrane (b) is shown in Fig. 6(b)).

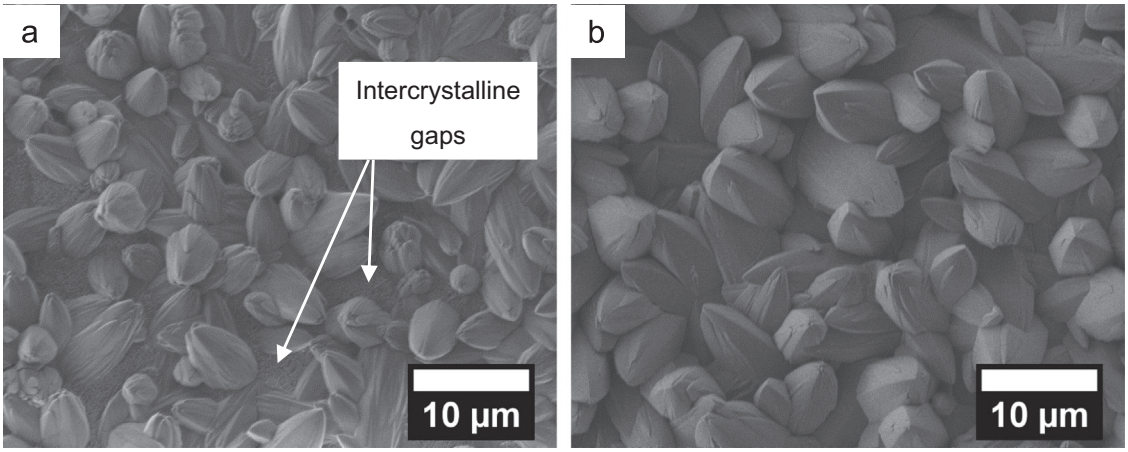

Fig. 3. Top view SEM images of Mg-MOF-74 membranes prepared (a) directly on the α-Al_2O_3 support and (b) on MgO-seeded α-Al_2O_3 support at 120 °C for 24 h.

the alumina substrate surface with MgO seeds, which are expected to promote both nucleation and growth of the Mg-MOF-74 layer. As shown in Fig. 3(b), the membranes prepared on MgO-seeded α-Al_2O_3 supports are indeed dense and no inter-crystalline voids can be observed. In the present work, MgO powders (< 50 nm) were coated on the surface of the support with the help of PEI, and served as nucleation centers which released Mg^{2+} ions into the synthesis solution, thus promoting the following growth of the Mg-MOF-74 crystals. After the synthesis of the membranes, the MgO seeds have transformed fully into the Mg-MOF-74. On the one hand, we cannot see any MgO seeds from the cross-section view of the membrane. On the other hand, the XRD patterns (Fig. 4) also indicate that the peaks of MgO disappeared after the membrane was grown on the support. Before choosing the MgO as seeds, we have also tried using Mg-MOF-74 nano crystals as seeds. However, these membrane preparations on the Mg-MOF-74-seeded supports, either by seeding in DMF or in ethanol, were not successful. The crystals grew too fast to large 10 μm sized crystals, and intercrystalline cracks were unavoidable.

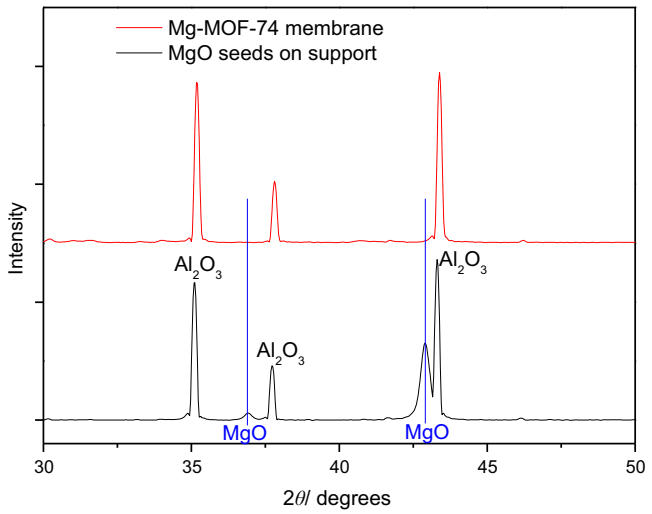

Fig. 4. XRD patterns of MgO seeds on the Al_2O_3 support and synthesized Mg-MOF-74 membranes.

3.2. *Effects of the synthesis time*

With the secondary growth method, the effect of the synthesis time on the membrane microstructure was followed. Fig. 5 shows SEM images of the Mg-MOF-74 membranes prepared on MgO-seeded α-Al_2O_3 supports for different synthesis times at 120 °C. As shown in Fig. 5(a), after 12 h, the alumina support surface has been covered by separate Mg-MOF-74 crystals. As the synthesis time increases to 20 h, more Mg-MOF-74 crystals are attached to the substrate and gradually form a thin and continuous layer, although there are still observable inter-crystalline gaps between the Mg-MOF-74 crystals (Fig. 5(b)). A dense Mg-MOF-74 membrane can be formed if the synthesis time increases up to 24 h. It can be seen that the support surface was completely covered by

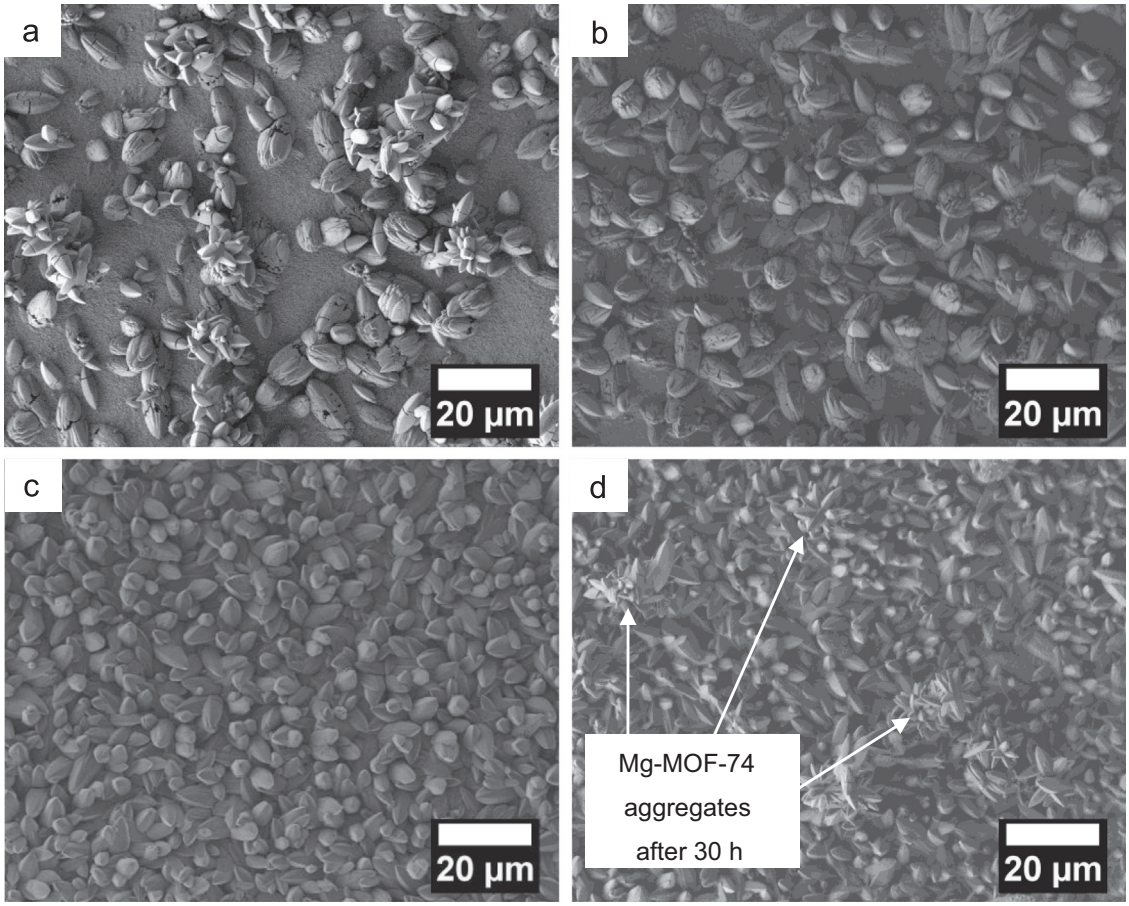

Fig. 5. Top view SEM images of Mg-MOF-74 membranes prepared on MgO-seeded α-Al_2O_3 supports at 120 °C for different synthesis times: (a) 16 h, (b) 20 h, (c) 24 h and (d) 30 h (for the XRD see Fig. 6).

uniform Mg-MOF-74 crystals with a grain size of about 10 μm, and no cracks or other macroscopic defects are visible (Fig. 5(c)). By further extending the synthesis time to 30 h, more Mg-MOF-74 crystals agglomerate on the as-prepared membrane, resulting in a rough membrane surface (Fig. 5(d)). The evolution of the Mg-MOF-74 membrane formation is also characterized by XRD, as shown in Fig. 6, compared with the XRD patterns of Mg-MOF-74 powder (Fig. 6(a)). After an elapse of 16 h, the first peaks of the Mg-MOF-74 crystals have been detected on the support surface (Fig. 6(b)). The heights of the Mg-MOF-74 diffraction peaks relative to the α-Al_2O_3 support increase with synthesis time, which indicates that the thickness of the membrane increases with time. After 24 h, the heights of the Mg-MOF-74 peaks relative to the α-Al_2O_3 support remain unchanged, which indicates that the Mg-MOF-74 crystals completely have covered the surface of the substrate (Fig. 6e). We conclude therefore, that 24 h at 120 °C is the optimum synthesis condition for the preparation of Mg-MOF-74 membranes.

Unfortunately, in this special case, it is impossible to draw from the XRD any conclusions about the crystal and – therefore – channel orientation in the membrane by simply comparing the XRD patterns of the isotropic powder and the membrane (Fig. 6(a) and (e)). This is due to the fact that all dominant peaks in the powder XRD pattern can be allocated to Miller indices (−1 2 0), (0 3 0) and (−1 5 0) with l values of 0. Therefore, the formation of a "crystallographic preferred orientation" (CPO) index (Jeong et al., 2002) gives no information on the channel orientation in l direction. It has to be mentioned, that our XRD of the supported Mg-MOF-74 is similar to the XRD of Ni-MOF-74 and Zn-MOF-74 grown on alumina support (Bétard et al., 2010).

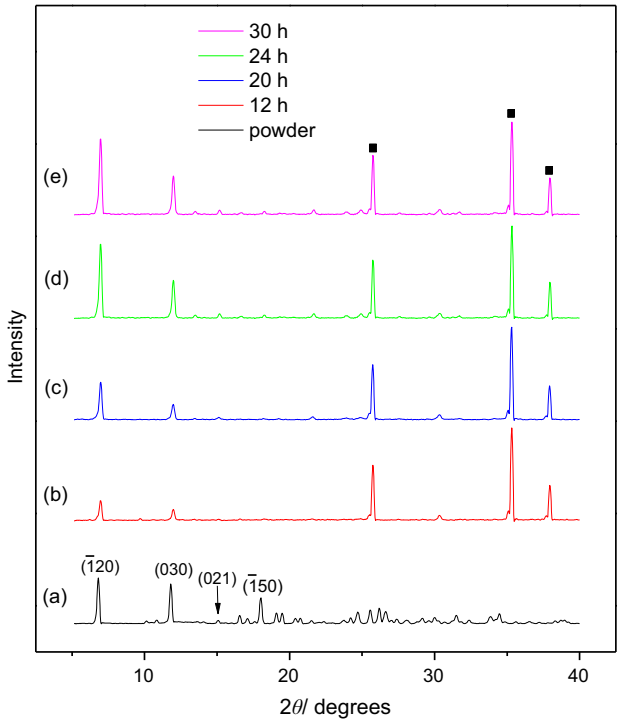

Fig. 6. XRD patterns of Mg-MOF-74 membranes prepared on MgO-seeded α-Al_2O_3 supports at 120 °C for different synthesis times: (b) 16 h, (c) 20 h, (d) 24 h and (e) 30 h, compared with (a) the XRD patterns of Mg-MOF-74 powder. (■): Al_2O_3 support, (not marked): Mg-MOF-74 (for the SEM see Fig. 5).

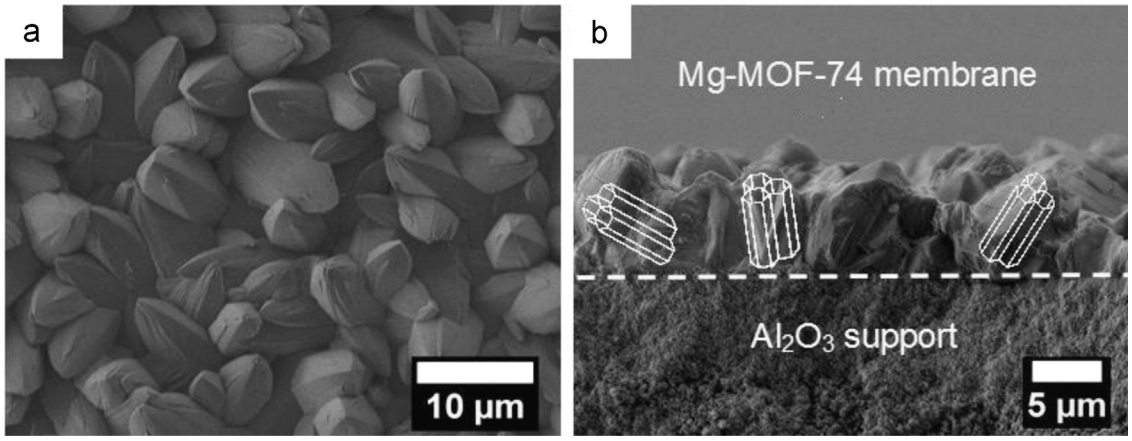

Fig. 7. (a) Top view and (b) cross-section SEM images of the Mg-MOF-74 membrane prepared on MgO-seeded α-Al_2O_3 supports at 120 °C for 24 h. The white channels in (b) stand for the orientation of the 1 D pores in Mg-MOF-74 crystals.

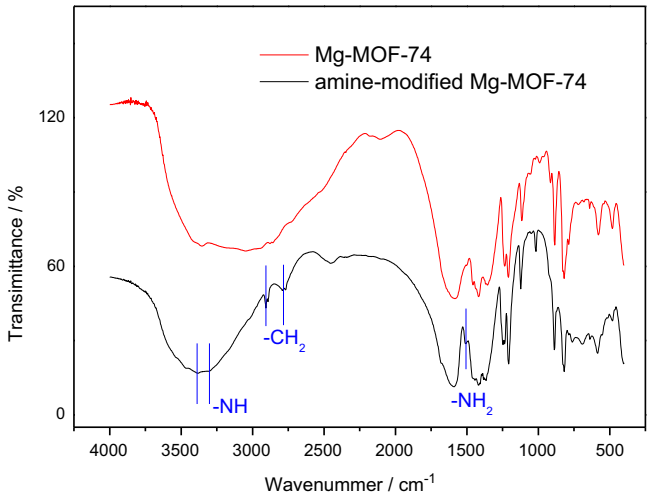

Fig. 8. FT-IR spectra of as-prepared and amine-modified Mg-MOF-74 crystals at room temperature.

Fig. 7 shows the Mg-MOF-74 membrane prepared on a MgO-seeded support for 24 h at 120 °C. From the cross-section view (Fig. 7(b)), the membrane is well intergrown with a thickness of about 10 μm. The shown membrane top view and the cross-section (Fig. 7) indicate that the crystals in the membrane show no statistical arrangement on the support but rather a tilted orientation with their trigonal axis perpendicular to the support. Thanks to this, a major part of all the 1D channels, which run along the *c*-axis of the trigonal structure, should be available for gas separation. Because of this tilted orientation of the *c*-axis, a huge amount of crystal planes and edges without an $l \neq 0$ value such as $(-1\ 2\ 0)$ and $(0\ 3\ 0)$ are present and dominate the XRD as another reason for the above mentioned problematic orientation determination via XRD.

3.3. Effects of the post-modification

The Mg-MOF-74 membranes prepared on MgO-seeded α-Al_2O_3 supports were then post-modified with ethylenediamine. Fig. 8 shows the FT-IR spectra of non-modified and ethylenediamine-modified Mg-MOF-74 membranes. Both two samples contain a broad band at around 3450 cm^{-1}, which can be assigned to O-H stretching vibrations of adsorbed water, and most of the bands in the region from about 1600 to 800 cm^{-1} are due to the stretching of the aromatic ring. Although lots of bands in the fingerprint region cannot be recognized clearly due to the overlapping of functional groups, some remarkable bands can still be distinguished. Compared with the FT-IR spectrum of non-modified Mg-MOF-74, the FT-IR spectrum of ethylenediamine-modified Mg-MOF-74 contains characteristic bands at 3370, 3285, 2932, 2814 and 1545 cm^{-1}, which match well with the FT-IR spectrum of ethylenediamine (Bétard et al., 2010; Su et al., 2010; Chang et al., 2003; Sabo et al., 2006). The bands shown at 3370, 3285 and 1545 cm^{-1} are related to NH_2 vibration in the primary amine group. The absorptions of the CH_2 groups of the aliphatic chains of ethylenediamine are observed at 2935 and 2814 cm^{-1} and are attributed to the asymmetric and symmetric stretching vibrations and deformation vibrations. The presence of $-NH_2$ and $-CH_2$ of the aliphatic chain after the amine modification confirms that ethylenediamine has been successfully grafted onto the Mg-MOF-74 crystals according to the recipe given in Choi et al. (2012). Judged by the SEM image and XRD pattern (not shown here), both the morphology and structure of the Mg-MOF-74 membrane remain unchanged after the amine-modification.

3.4. Results of single gas permeation and mixture gas separation

The single gas permeances on the as-prepared and amine-modified Mg-MOF-74 membranes at 25 °C and 1 bar as a function of the kinetic diameter of the gas molecules are shown in Fig. 9, and the inset gives the mixture separation factors for H_2 over other gases from their equimolar mixtures. The single gas permeances and ideal separation factors are summarized in Table 1, and the permeation data for mixed gases are listed in Table 2.

It follows from Fig. 9 to Table 1 that the single gas permeances of the as-prepared Mg-MOF-74 membrane follow the order: $H_2 > CH_4 > N_2 > CO_2$, with a H_2 permeance of 1.2×10^{-7} mol m^{-2} s^{-1} Pa^{-1}. The mixture separation factor of H_2/CO_2 with 10.5 is much higher than those of H_2/CH_4 (5.4) and H_2/N_2 (3.8) (inset in Fig. 9). This surprising experimental finding can be described by the diffusivity-solubility model of permeation (Krishna and van Baten, 2011). According to the rough estimate "permeation selectivity = adsorption selectivity x diffusion selectivity", a strong CO_2 adsorption over H_2 could lead to a CO_2-selective membrane. As reported previously (Yazaydin et al., 2009), Mg-MOF-74 shows very high CO_2 capture ability due to the unsaturated Mg^{2+} site, thus CO_2 can be stored in the pore structure Mg-MOF-74 especially. However, this strong CO_2 adsorption reduces the CO_2 mobility over proportional so that the Mg-MOF-74 membrane shows by the end a H_2 over CO_2 selectivity.

It is known that CO_2 interacts electronically also with amines (Langeroudi et al., 2009; Serna-Guerrero et al., 2008; Planas et al., 2013). It was our concept, therefore, to further enhance the H_2/CO_2 selectivity by increasing the adsorptive interaction of CO_2 by

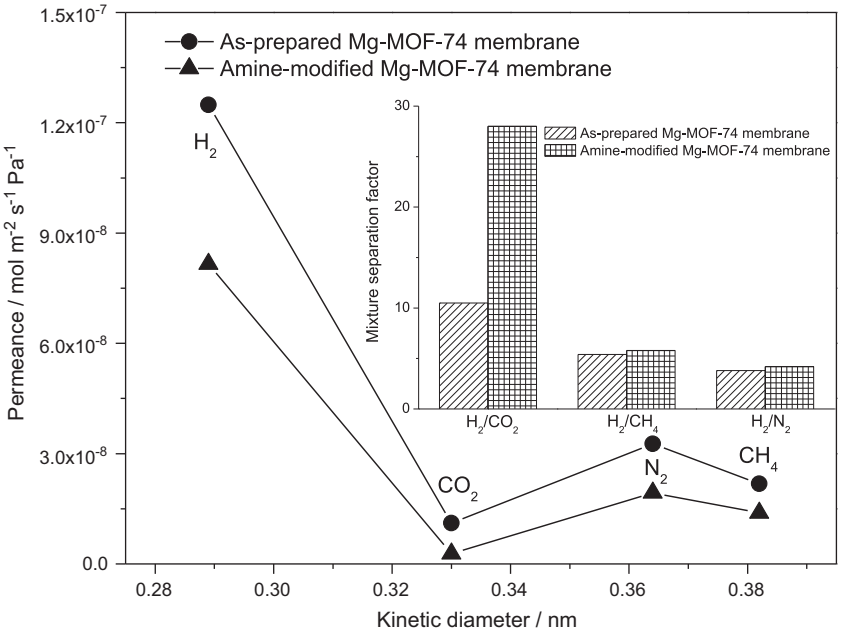

Fig. 9. Single gas permeances on the as-prepared and amine-modified Mg-MOF-74 membranes at 25 °C and 1 bar as a function of the kinetic diameter. The inset shows the mixture separation factors for H_2 over other gases from equimolar mixtures (for the temperature dependence of the H_2/CO_2 mixed gas selectivities see Fig. 10).

Table 1
Single gas permeation performances of the as-prepared and amine-modified Mg-MOF-74 membrane at 25 °C and 1 bar.

$Gas_{i/j}$	KC*	As-prepared Mg-MOF-74 membrane			Amine-modified Mg-MOF-74 membrane		
		Permeances (i) (mol m^{-2} s^{-1} Pa^{-1})	Permeances (j) (mol m^{-2} s^{-1} Pa^{-1})	Ideal separation factor	Permeances (i) (mol m^{-2} s^{-1} Pa^{-1})	Permeances (j) (mol m^{-2} s^{-1} Pa^{-1})	Ideal separation factor
H_2/CO_2	4.7		1.1×10^{-8}	11		2.8×10^{-9}	29
H_2/CH_4	2.8	1.24×10^{-7}	2.2×10^{-8}	5.6	8.2×10^{-8}	1.4×10^{-8}	5.8
H_2/N_2	3.7		3.5×10^{-8}	3.5		1.9×10^{-8}	4.3

* KC: Knudsen constant.

Table 2
Mixed gas separation performances of the as-prepared and amine-modified Mg-MOF-74 membrane at 25 °C and 1 bar with 1:1 binary mixtures.

$Gas_{i/j}$	KC*	As-prepared Mg-MOF-74 membrane			Amine-modified Mg-MOF-74 membrane		
		Permeances (i) (mol m^{-2} s^{-1} Pa^{-1})	Permeances (j) (mol m^{-2} s^{-1} Pa^{-1})	Mixture separation factor	Permeances (i) (mol m^{-2} s^{-1} Pa^{-1})	Permeances (j) (mol m^{-2} s^{-1} Pa^{-1})	Mixture separation factor
H_2/CO_2	4.7	1.0×10^{-7}	9.8×10^{-9}	10.5	7.6×10^{-8}	2.7×10^{-9}	28
H_2/CH_4	2.8	1.1×10^{-7}	2.1×10^{-8}	5.4	7.5×10^{-8}	1.3×10^{-8}	5.8
H_2/N_2	3.7	1.2×10^{-7}	3.3×10^{-9}	3.8	7.6×10^{-8}	1.8×10^{-8}	4.2

* KC: Knudsen constant.

amine-modification of prepared Mg-MOF-74 membrane. As expected, after the amine-modification, due to the narrowed pore size of MOF-74 the single gas permeances of H_2, CH_4 and N_2, decreased slightly by only a factor of 1.5, 1.6, and 1.8, respectively. However, the CO_2 permeance has been reduced by a factor of 4 from 1.1×10^{-8} mol m^{-2} s^{-1} Pa^{-1} to 2.8×10^{-9} mol m^{-2} s^{-1} Pa^{-1}. As a result, the mixed separation factors of H_2 against CH_4 and N_2 remained almost unchanged after the amine-functionalization, but the mixture separation factor of H_2/CO_2 dramatically increased from 10.5 to 28.

Due to the large pore size of about 11 Å, the size-based molecular sieve effect of Mg-MOF-74 was negligible. After the amine-modification, the pore size of the membrane was narrowed, but the pores are still large enough for the passage of small molecules like H_2, CH_4, N_2 and CO_2. Therefore, the mixture separation factors of H_2/CH_4 and H_2/N_2 do not change much when the membrane is modified by the diamine. On the contrary, the surface modification with amine groups has enhanced the strong adsorption of CO_2 molecules, which in turn reduces the permeance of CO_2, leading to an increase of the separation performance of H_2 over CO_2. As reported previously (Choi et al., 2012), one side of the amine group of ethylenediamine is bound to the open coordination sites of the Mg in the framework structure by direct ligation, while the amine group on the other side remains free in space (Hwang et al., 2008). Fig. 10 shows the mixture separation factors for equimolar H_2/CO_2 mixtures and the single

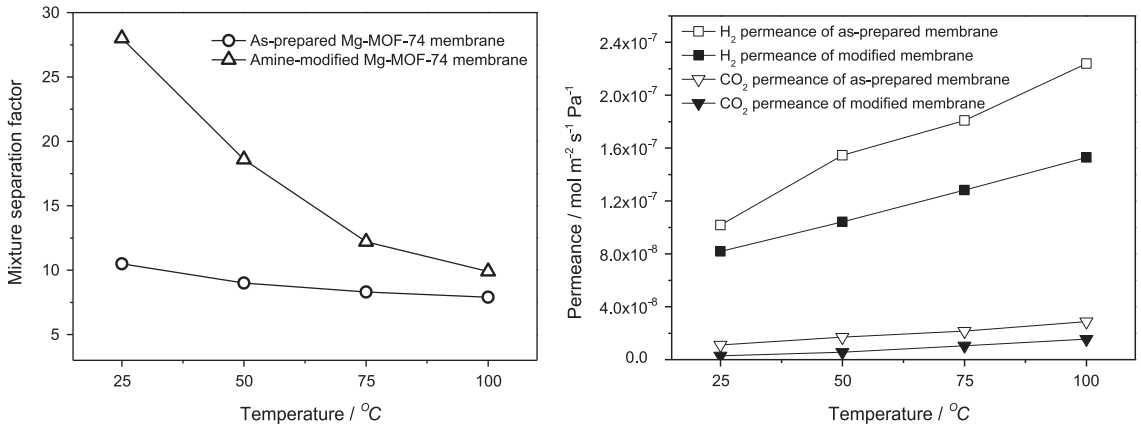

Fig. 10. Mixture separation factors for H_2/CO_2 from equimolar mixture (left) and single gas permeances of H_2 and CO_2 (right) on the as-prepared and amine-modified Mg-MOF-74 membranes at 1 bar as a function of temperature.

Table 3
Activation energies of H_2 and CO_2 permeation for Mg-MOF-74 membrane before and after amine-modification.

	Activation energy E_{act} (kJ mol^{-1})
H_2 before amine-modification	7.65
H_2 after amine-modification	7.71
CO_2 before amine-modification	11.4
CO_2 after amine-modification	20.9

gas permeances of H_2 and CO_2 on the as-prepared and amine-modified Mg-MOF-74 membranes at 1 bar as a function of temperature from 25 to 100 °C. For both the as-synthesized and amino-functionalized Mg-MOF-74 membranes the separation factors reduce gradually with increasing temperature. However, the reduction of the separation factors for the modified Mg-MOF-74 membrane was more remarkable since rising temperature has reduced the preferential adsorption of CO_2 on the amine groups. This trend is a good argument, that the interplay of adsorption and diffusion dominates the gas separation performance, rather than the size-based molecular sieving mechanism. As temperature increases, less CO_2 becomes adsorbed and more gas molecules can go through in the resulting free volume, leading to an increase in the hydrogen permeance and a reduction of the H_2/CO_2 selectivity. The grafted ethylenediamine was also proven to be stable at 100 °C, since the heating process of 1 °C min^{-1} from 25 to 100 °C is also reversible. The apparent activation energies E_{act} for H_2 and CO_2 permeation before and after modification, which are shown in Table 3, were obtained by fitting the data between 25 and 100 °C. Whereas the activation energy of H_2 permeation remains unchanged by the amination process, the activation energy of CO_2 has been almost doubled. This experimental finding can be explained by both steric effects (pore narrowing) and energetic effects (amine-CO_2 interaction). Our activation energies of H_2 and CO_2 permeation are similar to literature data of other microporous membranes for H_2/CO_2 separation, like CVD modified DDR zeolite membrane developed by Kanezashi et al. (2008) (the activation energy for H_2 and CO_2 are 9.62 and 12.8, respectively), but different to CVI modified silica membrane by Koutsonikolasa et al. (2009) (the activation energy for H_2 and CO_2 are 15.8 and 7.4, respectively).

As shown in a Robeson plot (Robeson 1991; Robeson 2008) in Fig. 11, the H_2/CO_2 selectivities and H_2 permeances of both the as-synthesized and the amine-modified Mg-MOF-74 membranes exceed by far the "upper-bound" for polymeric membranes, and the H_2/CO_2 selectivity after amine-modification increases with

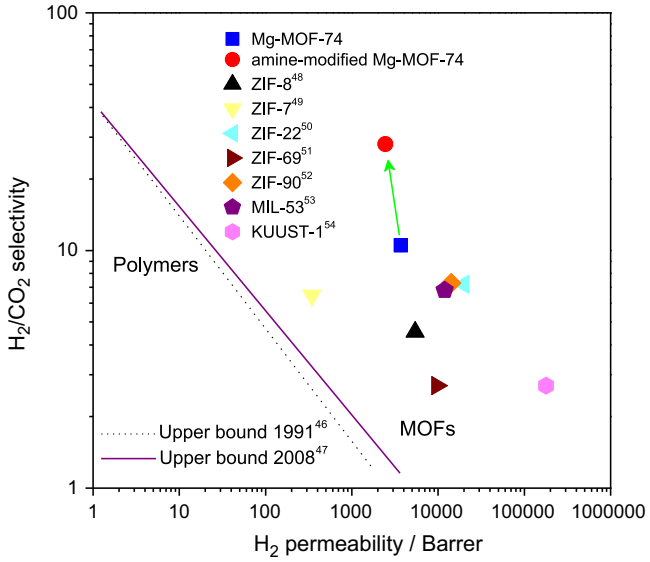

Fig. 11. H_2/CO_2 selectivity versus H_2 permeability for as-prepared and amine-modified Mg-MOF-74 membranes at 25 °C and 1 bar, compared with the previously reported MOF membranes. The upper bound lines for polymeric membranes are based on Robeson (1991) and Robeson (2008).

only a slight decrease of the permeability. Furthermore, also compared with other MOF membranes, our amine-modified MOF-74 membrane is a promising material for the H_2/CO_2 separation (Fig. 11 and Table 4). As shown in Fig. 11, compared with the existing polymer membranes, the amine-modified MOF-74 membrane exhibits a both much higher H_2/CO_2 selectivity and H_2 permeability which recommends amine-modified MOF-74 powder also a promising candidate for the preparation of mixed matrix membranes (MMM) (Mahajan and Koros, 2000). The MMM concept avoids the difficulty to prepare and scale up pure supported MOF membranes and can be produced more easily as spiral wound or hollow fiber module, compared to the pure MOF membranes.

As a proof of the good reproducibility of the MgO-seeding synthesis method and amine-modification, Table 5 shows the results of gas permeation performance for four tested amine-modified Mg-MOF-74 membranes prepared following identical synthesis method. The selectivities of H_2/CO_2 and H_2 and CO_2 permeance at room temperature do not scatter more than $\pm$10%, which indicates the good reproducibility of the Mg-MOF-74 membranes.

Table 4
H_2/CO_2 selectivity versus H_2 permeability for as-prepared and amine-modified Mg-MOF-74 membranes at 25 °C and 1 bar, compared with the previously reported MOF membranes.

MOF membranes	Thickness (μm)	H_2 permeance (mol m^{-2} s^1 Pa^1)	H_2 permeability* (Barrer)	H_2/CO_2 selectivity	References
Mg-MOF-74	10	1.2×10^{-07}	3.7×10^3	10.5	This study
Amine-modified Mg-MOF-74	10	8.2×10^{-08}	2.5×10^3	28	This study
ZIF-8	30	6.0×10^{-08}	5.4×10^3	4.5	Bux et al. (2009)
ZIF-7	1.5	7.7×10^{-08}	3.5×10^2	6.5	Li et al. (2010)
ZIF-22	40	1.7×10^{-07}	2.0×10^4	7.2	Huang et al. (2010)
ZIF-69	50	6.5×10^{-08}	9.7×10^3	2.7	Liu et al. (2010)
ZIF-90	20	2.4×10^{-07}	1.4×10^4	7.3	Huang et al. (2010)
MIL-53	8	5.0×10^{-07}	1.2×10^4	6.8	Hu et al. (2011)
KUUST-1	60	1.0×10^{-06}	1.8×10^5	2.7	Guo et al. (2009)

* Permeability is calculated as the membrane permeance multiplied by the membrane thickness. 1 Barrer = 3.348×10^{-16} mol m/(m^2 s Pa).

Table 5
Gas permeances of H_2 and CO_2 and mixture separation factors of H_2/CO_2 from equimolar mixtures at room temperature and 1 bar of 4 tested Mg-MOF-74 membranes.

	H_2 permeance (mol m^{-2} s^{-1} Pa^{-1})	CO_2 permeance (mol m^{-2} s^{-1} Pa^{-1})	Mixture separation factor H_2/CO_2
1	8.2×10^{-8}	2.8×10^{-9}	28
2	9.0×10^{-8}	3.1×10^{-9}	30
3	7.4×10^{-8}	2.8×10^{-9}	25
4	7.5×10^{-8}	2.9×10^{-9}	26

4. Conclusion

Phase-pure and compact Mg-MOF-74 membranes have been prepared successfully on MgO-seeded porous Al_2O_3 supports at 120 °C for 24 h after optimization of the synthesis solution. The mixture separation factor of H_2/CO_2 was much higher than those of H_2/CH_4 and H_2/N_2, especially at lower temperature. After amine-functionalization of the Mg-MOF-74 membrane by using ethylenediamine, the separation performance of H_2/CO_2 was remarkably enhanced and the mixture separation performance increased from 10.5 to 28 at room temperature. This increase is ascribed to two effects: (i) One amino group of the diamine is docked to the open Mg site, thus the diamine narrows the effective pore size which retards for steric reasons the carbon dioxide (kinetic diameter 3.3 Å) permeation stronger than the hydrogen one (2.9 Å), and (ii) the other amino group interacts with CO_2 thus reducing its mobility.

Acknowledgements

Financial support by EU CARENA (FP7-NMP-2010-LARGE-4, Nr. 263007), and Chinese Academy of Science Visiting Professorship for Senior International Scientists (Grant No. 2013T1G0047) is acknowledged.

References

Arnold, M., Kortunov, P., Jones, D., Nedellec, Y., Kärger, J., Caro, J., 2007. Oriented crystallization on supports and anisotropic mass transport of the metal organic framework manganese formate. Eur. J. Inorg. Chem. 1, 60–64.
Bae, T., Long, J.R., 2013. CO2/N2 separations with mixed-matrix membranes containing Mg2(dobdc) nanocrystals. Energy Environ. Sci. 6, 3565–3569.
Bétard, A., Zander, D., Fischer, R.A., 2010. Dense and homogeneous coatings of CPO-27-M type metal–organic frameworks on alumina substrates. CrystEngComm 12, 3768–3772.
Böhme, U., Barth, B., Paula, C., Kuhnt, A., Schwieger, W., Mundstock, A., Caro, J., 2013. Martin Hartmann, Ethene/ethane and propene/propane separation via the olefin and paraffin selective metal–organic framework adsorbents CPO-27 and ZIF-8. Langmuir 29, 8592–8600.
Britt, D., Furukawa, H., Wang, B., Glover, T.G., Yaghi, O.M., 2009. Highly efficient separation of carbon dioxide by a metal–organic framework replete with open metal sites. Proc. Natl. Acad. Sci. 106, 20637–20640.
Brown, A.J., Brunelli, N.A., Eum, K., Rashidi, F., Johnson, J.R., Koros, W.J., Jones, C.W., Nair, S, 2014. Interfacial microfluidic processing of metal–organic framework hollow fiber membranes. Science 345, 72–75.
Bux, H., Liang, F., Li, Y., Cravillon, J., Wiebcke, M., Caro, J., 2009. Zeolitic imidazolate framework membrane with molecular sieving properties by microwave-assisted solvothermal synthesis. J. Am. Chem. Soc. 131, 16000–16001.
Caskey, S.R., Wong-Foy, A.G., Matzger, A.J., 2008. Dramatic tuning of carbon dioxide uptake via metal substitution in a coordination polymer with cylindrical pores. J. Am. Chem. Soc. 130, 10870–10871.
Chang, A.C.C., Chuang, S.S.C., Gray, M., Soong, Y., 2003. In-situ infrared study of CO2 adsorption on SBA-15 grafted with gamma-(aminopropyl)triethoxysilane. Energy Fuels 17, 468–473.
Choi, S., Watanabe, T., Bae, T., Sholl, D.S., Jones, C.W., 2012. Modification of the Mg/DOBDC MOF with amines to enhance CO2 adsorption from ultradilute gases. J. Phys. Chem. Lett. 3, 1136–1141.
de Vos, R.M., Verweij, H., 1998. High-selectivity, high-flux silica membranes for gas separation. Science 279, 1710–1711.
Dietzel, P.D.C., Besikiotis, V., Blom, R., 2009. Application of metal–organic frameworks with coordinatively unsaturated metal sites in storage and separation of methane and carbon dioxide. J. Mater. Chem. 19, 7362–7370.
Dietzel, P.D.C., Georgiev, P.A., Eckert, J., Blom, R., Strässle, T., Unruh, T., 2010. Interaction of hydrogen with accessible metal sites in the metal–organic frameworks M2(dhtp) (CPO-27-M; M=Ni, Co, Mg). Chem. Commun. 46, 4962–4964.
Dietzel, P.D.C., Johnsen, R.E., Blom, R., Fjellvag, H., 2008. Structural changes and coordinatively unsaturated metal atoms on dehydration of honeycomb analogous microporous metal–organic frameworks. Chem. A Eur. J. 14, 2389–2397.
Dietzel, P.D.C., Morita, Y., Blom, R., Fjellvag, H., 2005. An in situ high-temperature single-crystal investigation of a dehydrated metal–organic framework compound and field-induced magnetization of one-dimensional metaloxygen chains. Angew. Chem. Int. Ed. 44, 6354–6358.
Dietzel, P.D.C., Panella, B., Hirscher, M., Blom, R., Fjellvag, H., 2006. Hydrogen adsorption in a nickel based coordination polymer with open metal sites in the cylindrical cavities of the desolvated framework. Chem. Commun. 9, 959–961.
Dzubak, A.L., Lin, L., Kim, J., Swisher, J.A., Poloni, R., Maximoff, S.N., Smit, B., Gagliardi, L., 2012. Ab initio carbon capture in open-site metal–organic frameworks. Nat. Chem. 4, 810–816.
Guo, H., Zhu, G., Hewitt, I.J., Qiu, S., 2009. "Twin copper source" growth of metal–organic framework membrane: Cu3(BTC)2 with high permeability and selectivity for recycling H2. J. Am. Chem. Soc. 131, 1646–1647.
Herm, Z.R., Krishna, R., Long, J.R., 2012. CO2/CH4, CH4/H2 and CO2/CH4/H2 separations at high pressures using Mg2(dobdc). Microporous Mesoporous Mater. 151, 481–487.
Hermes, S., Schroder, F., Chelmowski, R., Woll, C., Fischer, R.A., 2005. Selective nucleation and growth of metal–organic open framework thin films on patterned COOH/CF3-terminated self-assembled monolayers on Au(111). J. Am. Chem. Soc. 127, 13744–13745.
Hong, M., Li, S., Falconer, J.L., Noble, R.D., 2008. Hydrogen purification using a SAPO-34 membrane. J. Membr. Sci. 307, 277–283.
Hu, Y., Dong, X., Nan, J., Jin, W., Ren, X., Xu, N., Lee, Y.M., 2011. Metal–organic framework membranes fabricated via reactive seeding. Chem. Commun. 47, 737–739.
Huang, A., Bux, H., Steinbach, F., Caro, J., 2010. Molecular-sieve membrane with hydrogen permselectivity: ZIF-22 in LTA topology prepared with 3-aminopropyltriethoxysilane as covalent linker. Angew. Chem. Int. Ed. 49, 4958–4961.
Huang, A., Dou, W., Caro, J., 2010. Steam-stable zeolitic imidazolate framework ZIF-90 membrane with hydrogen selectivity through covalent functionalization. J. Am. Chem. Soc. 132, 15562–15564.
Huang, A., Liang, F., Steinbach, F., Caro, J., 2010. Preparation and separation properties of LTA membranes by using 3-aminopropyltriethoxysilane as covalent linker. J. Membr. Sci. 350, 5–9.

Huang, A., Wang, N., Kong, C., Caro, J., 2012. Organosilica-functionalized zeolitic imidazolate framework ZIF-90 membrane with high gas-separation performance. Angew. Chem. Int. Ed. 51, 10551–10555.
Hwang, Y.K., Hong, D.Y., Chang, J.S., Jhung, S.H., Seo, Y.K, Kim, J., Vimont, A., Daturi, M., Serre, C., Ferey, G., 2008. Amine grafting on coordinatively unsaturated metal centers of MOFs: consequences for catalysis and metal encapsulation. Angew. Chem. Int. Ed. 47, 4144–4148.
Jeong, H.K., Krohn, J., Sujaoti, K., Tsapatsis, M., 2002. Oriented molecular sieve membranes by heteroepitaxial growth. J. Am. Chem. Soc. 124, 12966–12968.
Kanezashi, M., O' Brien-Abraham, J., Lin, Y.S., Suzuki, K., 2008. Gas permeation through DDR-type zeolite membranes at high temperatures. AIChE J. 54, 1478–1486.
Kong, X., Scott, E., Ding, W., Mason, J.A., Long, J.R., Reimer, J.A., 2012. CO2 dynamics in a metal–organic framework with open metal sites. J. Am. Chem. Soc. 134, 14341–14344.
Koutsonikolasa, D., Kaldisb, S., Sakellaropoulos, G.P., 2009. A low-temperature CVI method for pore modification of sol–gel silica membranes. J. Membr. Sci. 342, 131–137.
Krishna, R., van Baten, J.M., 2011. In silico screening of metal–organic frameworks in separation applications. Phys. Chem. Chem. Phys. 13, 10593–10616.
Langeroudi, E.G., Kleitz, F., Iliuta, M.C., Larachi, F., 2009. Grafted amine/CO2 interactions in (Gas-)liquid–solid adsorption/absorption equilibria. J. Phys. Chem. C 113 (52), 21866–21876.
Lee, D., Li, Q., Kim, H., Lee, K., 2012. Preparation of Ni-MOF-74 membrane for CO2 separation by layer-by-layer seeding technique. Microporous Mesoporous Mater. 163, 169–177.
Li, Y., Bux, H., Feldhoff, A., Li, G., Yang, W., Caro, J., 2010. Controllable synthesis of metal–organic frameworks: from MOF nanorods to oriented MOF membranes. Adv. Mater. 22, 3322–3326.
Li, Y., Liang, F., Bux, H., Feldhoff, A., Yang, W., Caro, J., 2010. Molecular sieve membrane: supported metal–organic framework with high hydrogen selectivity. Angew. Chem. Int. Ed. 49, 548–551.
Li, Y., Liang, F., Bux, H., A., Yang, W., Caro, J., 2010. Zeolitic imidazolate framework ZIF-7 based molecular sieve membrane for hydrogen separation. J. Membr. Sci. 354, 48–54.
Liu, Q., Wang, N., Caro, J., Huang, A., 2013. Bio-inspired polydopamine: a versatile and powerful platform for covalent synthesis of molecular sieve membranes. J. Am. Chem. Soc. 135, 17679–17682.
Liu, Y., Hu, E., Khan, E.A., Lai, Z., 2010. Synthesis and characterization of ZIF-69 membranes and separation for CO2/CO mixture. J. Membr. Sci. 353, 36–40.
Lu, G., Hupp, J.T., 2010. Metal–organic frameworks as sensors: a ZIF-8 based Fabry–Perot device as a selective sensor for chemical vapors and gases. J. Am. Chem. Soc. 132, 7832–7833.
Mahajan, R., Koros, W.J., 2000. Factors controlling successful formation of mixed-matrix gas separation materials. Ind. Eng. Chem. Res. 39, 2692–2696.
Mason, J.A., Sumida, K., Herm, Z.R., Krishna, R., Long, J.R., 2011. Evaluating metal–organic frameworks for post-combustion carbon dioxide capture via temperature swing adsorption. Energy Environ. Sci. 4, 3030–3040.
Mundstock, A., Böhme, U., Barth, B., Hartmann, M., Caro, J., 2013. Propylene/propane separation in fixed-Bed adsorber and membrane permeation. Chem. Ing. Tech. 85, 1694–1699.
Ockwig, N.W., Nenoff, T.M., 2007. Membranes for hydrogen separation. Chem. Rev. 107, 4078–4110.
Planas, N., Dzubak, A.L., Poloni, R., Chiang, L., McManus, A., McDonald, T.M., Neaton, J.B., Lange, J.R., Smit, B., Gagliardi, L., 2013. The mechanism of carbon dioxide adsorption in an alkylamine-functionalized metal–organic framework. J. Am. Chem. Soc. 135, 7402–7405.
Ranjan, R., Tsapatsis, M., 2009. Microporous metal organic framework membrane on porous support using the seeded growth method. Chem. Mater. 21, 4920–4924.
Remy, T., Peter, S.A., Van der Perre, S., Valvekens, P., de Vos, D.E., Baron, G.V., Denayer, J.F.M., 2013. Selective dynamic CO2 separations on Mg-MOF-74 at low pressures: a detailed comparison with 13X. J. Phys. Chem. C 117, 9301–9310.
Robeson, L.M., 1991. Correlation of separation factor versus permeability for polymeric membranes. J. Membr. Sci. 62, 165–185.
Robeson, L.M., 2008. The upper bound revisited. J. Membr. Sci. 320, 390–400.
Rodenas, T., van Dalen, M., García-Pérez, E., Serra-Crespo, P., Zornoza, B., Kapteijn, F., Gascon, J., 2014. Visualizing MOF mixed matrix membranes at the nanoscale: towards structure-performance relationships in CO2/CH4 separation over NH2-MIL-53(Al)@PI. Adv. Funct. Mater. 24, 249–256.
Rosi, N.L., Kim, J., Eddaoudi, M., Chen, B.L., O'Keeffe, M., Yaghi, O.M., 2005. Rod packings and metal–organic frameworks constructed from rod-shaped secondary building units. J. Am. Chem. Soc. 127, 1504–1518.
Rostrup-Nielsen, J.R., Rostrup-Nielsen, T., 2002. Large-scale hydrogen production. CATTECH 6, 150–159.
Sabo, M., Boehlmannb, W., Kaskel, S., 2006. Titanium terephthalate (TT-1) hybrid materials with high specific surface area. J. Mater. Chem. 16, 2354–2357.
Seo, J.S., Whang, D., Lee, H., Jun, S.I., Oh, J., Jeon, Y.J., Kim, K., 2000. A homochiral metal–organic porous material for enantioselective separation and catalysis. Nature 404, 982–986.
Serna-Guerrero, R., Da'na, E., Sayari, A., 2008. New insights into the interactions of CO2 with amine-functionalized silica. Ind. Eng. Chem. Res. 47, 9406–9412.
Shiflett, M.B., Foley, H.C., 1999. Ultrasonic deposition of high-selectivity nanoporous carbon membranes. Science 285, 1902–1905.
Su, F., Lu, C., Kuo, S., Zeng, W., 2010. Adsorption of CO2 on amine-functionalized Y-type zeolites. Energy Fuels 24, 1441–1448.
Uemiya, S., Matsuda, T., Kikuchi, E., 1991. Hydrogen permeable palladium-silver alloy membrane supported on porous ceramics. J. Membr. Sci. 56, 315–325.
Wicke, E., Kallenbach, R., 1941. Die Oberflächendiffusion von Kohlendioxyd in aktiven Kohlen 97, 135-151.
Yaghi, O.M., O'Keeffe, M., Ockwig, N.W., Chae, H.K., Eddaoudi, M., Kim, J., 2003. Reticular synthesis and the design of new materials. Nature 423, 705–714.
Yang, D., Cho, H., Kim, J., Yang, S., Ahn, W., 2012. CO2 capture and conversion using Mg-MOF-74 prepared by a sonochemical method. Energy Environ. Sci. 5, 6465–6473.
Yazaydin, A.Ö., Snurr, R.Q., Park, T., Koh, K., Liu, J., LeVan, M.D., Benin, A.I., Jakubczak, P., Lanuza, M., Galloway, D.B., Low, J.J., Willis, R.R., 2009. Screening of metal–organic frameworks for carbon dioxide capture from flue gas using a combined experimental and modeling approach. J. Am. Chem. Soc. 131, 18198–18199.
Yoo, Y., Lai, Z., Jeong, H., 2009. Fabrication of MOF-5 membranes using microwave-induced rapid seeding and solvothermal secondary growth. Microporous Mesoporous Mater. 123, 100–106.
Yu, J., Balbuena, P.B., 2013. Water effects on postcombustion CO2 capture in Mg-MOF-74. J. Phys. Chem. C 117 (7), 3383–3388.
Zhao, Z., Li, Z., Lin, Y., 2009. Adsorption and diffusion of carbon dioxide on metal–organic framework (MOF-5). Ind. Eng. Chem. Res. 48, 10015–10020.